



UNIVERSITY OF TWENTE.

MASTER'S THESIS

Electrochemical characterisation of silicon nanowires

Henriëtte van Dorp

November 9, 2010

Report number: 2010-6

Supervisors:

Prof. dr. Albert van den Berg

Prof. dr. Wilfred van der Wiel

Dr. Wouter Olthuis

Dr. Edwin T. Carlen

Contents

| | | |
|----------|--|-----------|
| 1 | Introduction | 5 |
| 1.1 | Preface | 5 |
| 1.2 | Background | 6 |
| 1.3 | Goals | 7 |
| 1.4 | Outline | 7 |
| 2 | Theory | 9 |
| 2.1 | Introduction | 9 |
| 2.2 | Electrolyte Oxide Semiconductor system | 9 |
| 2.3 | The site binding model | 10 |
| 2.3.1 | Bousse model | 11 |
| 2.3.2 | Van Hal model | 12 |
| 2.4 | ISFET | 15 |
| 2.4.1 | Previous work on ISFETs | 16 |
| 2.4.2 | Effect of monolayers | 16 |
| 2.5 | Silicon nanowires | 17 |
| 2.5.1 | Previous pH-measurements on SiNWs | 17 |
| 2.6 | Comparison ISFETs and SiNWs | 18 |
| 3 | Experimental | 19 |
| 3.1 | Introduction | 19 |
| 3.2 | The reference electrode | 19 |
| 3.3 | Silicon nanowire device structure | 19 |
| 3.4 | Methods | 20 |
| 3.4.1 | Packaging | 20 |
| 3.4.2 | Monolayers | 20 |
| 3.4.3 | Electrochemical measurements | 21 |
| 3.5 | Comparison ISFET method and SiNW method | 22 |
| 4 | Results and discussion | 23 |
| 4.1 | Introduction | 23 |
| 4.2 | Theoretical curves | 23 |
| 4.3 | Electrical measurements | 25 |
| 4.4 | pH measurements on bare SiO ₂ | 25 |
| 4.5 | Monolayer pH measurements | 25 |
| 4.5.1 | APTES functionalisation | 25 |
| 4.5.2 | HMDS functionalisation | 26 |

| | | |
|----------|---|-----------|
| 4.6 | Parameter extraction | 27 |
| 5 | Conclusion | 29 |
| A | Mathematica files | 31 |
| A.1 | Bousse model | 31 |
| A.2 | Van Hal and Gouy-Chapman theory | 32 |
| A.3 | Van Hal and Gouy-Chapman-Stern theory | 33 |
| B | List of parameters | 35 |
| | References | 37 |

Chapter 1

Introduction

1.1 Preface

When you near the end of the Electrical Engineering programme, there is only one thing left to do: graduating. In order to graduate, you have to write a thesis on a research subject. This means doing research all on your own, in one of the many EE chairs. So before you get to that point, it's time to choose which chair and most importantly, which subject.

For me, choosing was not too hard. The Biomedical Systems master track I followed had two main chairs, BSS (Biomedical signals and systems) and the BIOS Lab on a Chip group. I had done my bachelor thesis at BSS and during the master track my interest shifted from subjects from the BSS group to subjects from the BIOS group. After doing my internship under guidance of Edwin Carlen from the BIOS group, I knew for certain that I wanted to do my master's thesis there as well. Friendly, (almost) always available and with an interesting research subject: silicon nanowires. This subject was 'electrical engineering' enough for my taste and the wires seem like the next big thing in biosensors, so it piqued my interest. These tiny wires, how could they have nearly the same function, even more, as a much bigger ISFET? It was very intriguing, so I wanted to study them in more detail. And with the subject of Edwin Carlen, I could. My work on nanowires was to be done under daily supervision of Songyue Chen, a PhD-student who had already done her master's thesis on nanowires and was now working the same subject for her PhD.

A master's thesis is never really done all on your own, as people help you out with things, most of all your daily supervisors. These two people are therefore the first that I would like to thank for their help with my work, so Edwin and Songyue, thank you very much for the interesting discussions, the help with the labwork and kicking my butt when necessary. Johan Bommer, thank you for helping me while I was struggling with the wirebonder and JanN, thank you for cleaning my chips when Songyue wasn't around. I also thank the rest of the BIOS group for all the fun we had. Furthermore, I would like to thank Albert van den Berg, Wouter Olthuis and Wilfred van der Wiel for being my graduation committee.

My dad has read my entire thesis time and again to check for typos, grammar, mis-referencing and things that should have been explained better or go bump in the night, for which I am very grateful. A big thank you to my mum as well, who was there for support.

And last but not least, my boyfriend, Dirk-Jan, not only for support and coping with my moodswings, but also for being there for even the tiniest problems Songyue and I had concerning the Labview program and adding more and more to it whenever we wished for it.

1.2 Background

In the BIOS Lab on a Chip group, a lot of research has been done in the field of ion selective field effect transistors (ISFETs), ranging from inventing them [1] to characterisation [2, 3, 4] and more recently to silicon nanowires or nanoISFETs [5, 6]. The characterisation for ISFETs is now used for describing the electrical properties of silicon nanowire (SiNW) FETs [5, 7, 8] because the basic function of SiNW FETs and ISFETs are comparable.

Silicon nanowires provide a similar function to ISFETs, albeit on a different scale. The two connector-pads at the end of the wire will act like a source and drain, with the wire as the channel. However, the ISFET has source and drain from different doped material than the bulk, the entire nanowire is made from one type of material. The gating is also different, because the most commonly used ISFET is a n-channel enhancement mode device, which uses an inversion layer of minority carriers near the gate oxide/silicon interface with a gate electrode providing channel conduction from source to drain.

The nanowire is gated similarly to an ISFET, but the depletion layer, which is three dimensional instead of two, is modulated through field effect using frontgate voltage or through the buried oxide layer using backgate voltage instead of only frontgate field effect. Doped wires, or depletion mode, are most commonly gated using frontgate voltage, while undoped wires use backgate voltage. The last difference is that nanowires are majority carrier devices, whereas ISFETs are minority carrier devices.

Nanowires are fabricated in two ways, top down or bottom up. The top down fabricated nanowires also exist in two types: wide and flat, so a low w/h ratio, usually undoped, or higher but narrower, so a high w/h ratio, usually doped. The silicon nanowire used for the experiments in this thesis fall in this last category, top down depletion mode device with the width nearly the same as the height. The wire, which acts as the channel, is doped with an impurity (typically boron) and the gate electrode either depletes or accumulates the majority carriers near the silicon surface.

Applications of these nanowires can be found in literature. In the Charles Lieber group at Harvard, Cui used top down, p-type, boron doped bare SiO₂ and 3-aminopropyltriethoxysilane (APTES) modified SiNWs and did pH measurements on these in a microfluidic channel. The wires were ultimately used as a disease marker sensor using biotin-streptavidin binding [9]. In the same group, Zheng used sensor arrays made of multiplexed, electrically addressable silicon nanowires to detect prostate specific antigen. Patolsky used p-type SiNWs for real-time, label-free detection of virus molecules. Hahn used nanowires which were surface modified with avidin protein, to detect PNA-DNA hybridisation [10]. With Hewlett Packard, Li used top-down fabricated p-type SiNWs to detect single-stranded DNA with oligonucleotides and PNA probe molecules [10]. The James Heath group at California Institute of Technology uses top down, boron doped p-type silicon nanowires with APTES surface functionalisation as DNA sensors. [11]. At Yale, the group of Mark Reed uses 200 nm wide p-type undoped top down structures for detection of biotin-streptavidin and immunodetection using immunoglobulin proteins [12]. The Technische Universität München has devised a thin, broad nanowire device, using top-down fabrication and undoped material and used it for pH-measurements, comparing it to an ISFET theoretical model. At the University of Twente, more specifically the BIOS group, triangular top down, p-type, boron doped wires are used to sense pH and as a hypermethylated DNA detection device.

1.3 Goals

Surprisingly, very little research on nanowires like in München has been done to compare measurements of SiNWs to ISFETs. Most research uses a theoretical ISFET model with the same parameters as for the ISFETs. Therefore, a comparison of the theoretical model is needed between ISFETs and SiNWs. In order to test the model, experiments are needed to study the behaviour of the nanowires in solutions with different pH, to see the effect of protonation on the surface charge of the wire and to compare this to the vast literature available on ISFETs. This surface charge also depends on the type of surface groups on the oxide surface, which can be changed by adding a monolayer to the wire.

Because of this lack of research into the subject, it is a good topic for a Master's thesis. In this thesis, an answer to the following research questions will be sought:

- How do silicon nanowires compare to ISFETs?
- What is the behaviour of silicon nanowires in changing pH solution?
- Are the extended parameters that characterise the surface the same for ISFETs and SiNWs? If not, why?

1.4 Outline

After introducing the site binding model, to be used as a framework for the Theory Chapter, further detail as to the electrochemical properties of ion selective field effect transistors and silicon nanowires will be explained. The Chapter on experimental work will describe previous experimental work on ISFETs and SiNWs, as well as the setup and protocol for the experiments needed to answer the research questions. The outcome of those experiments can be found in the Results and discussion Chapter, where parameters are extracted from the results. The research questions are answered in the Concluding Chapter.

Chapter 2

Theory

2.1 Introduction

To answer the research questions, a model for the pH behaviour of silicon nanowires (SiNWs) should be set up to compare it with the ion sensitive field effect transistor (ISFET) model. As both the SiNWs and ISFETs are electrolyte oxide semiconductor systems, an introduction to this concept is given. Then the site binding model (SBM) is introduced, which is a model for proton binding to surface groups, often called site dissociation. The number of protons in a solution is a function of the pH of that solution, so the site dissociation is related to pH. The Bousse and Van Hal ISFET models will be introduced and compared to each other. They give a combination of the SBM and the Gouy-Chapman (GC) and Gouy-Chapman-Stern (GCS) model which both describe the ionic behaviour at the oxide surface. Combined with the electrolyte oxide semiconductor (EOS) system, these models can give insight to the electrical behaviour of ISFETs and SiNWs. A comparison of ISFETs and SiNWs concludes the Chapter.

2.2 Electrolyte Oxide Semiconductor system

The EOS system is used to describe the basic interaction of charge in an oxide with the charge in an electrolyte. The pH behaviour of the system is primarily dictated by this interface, and the semiconductor is used to measure the EO behaviour using an electric field across the oxide layer, hence the name field effect transistor (FET). The charge in the semiconductor depends on the surface potential ψ_0 of the oxide due to the surface charge density σ_0 .

Silicon field-effect devices like ISFETs and SiNWs have three operating regimes: accumulation, depletion and inversion, named after the space charge regions in the semiconductor layer that are created due to modification of the surface potential ψ_s of the silicon surface [13]. In the depletion regime, the bound ionised impurity charge Q_d dominates, in the accumulation and inversion regimes free charges at the surface dominate (Q_a and Q_i respectively) [13].

With gate voltage controlled devices in electrolyte, the EOS system (Figure 2.1a) describes the charge modulation behaviour. The reference electrode biases the solution electrically and creates an applied field at the silicon surface which changes the charge on the surface. Figure 2.1b shows the total silicon charge as a function of small variations of V_{fg} . The inset shows ψ_s as a function of the variations of V_{fg} . In the depletion region, ψ_s shows large variations for changes in V_{fg} , while in the accumulation and inversion region ψ_s only changes slightly for variations in V_{fg} , which means that device sensitivity is low in those regions. For negative V_{fg} , accumulation of majority carriers occurs which increases sharply with V_{fg} , more or less independent of the impurity doping concentration. For a small positive V_{fg} the silicon body

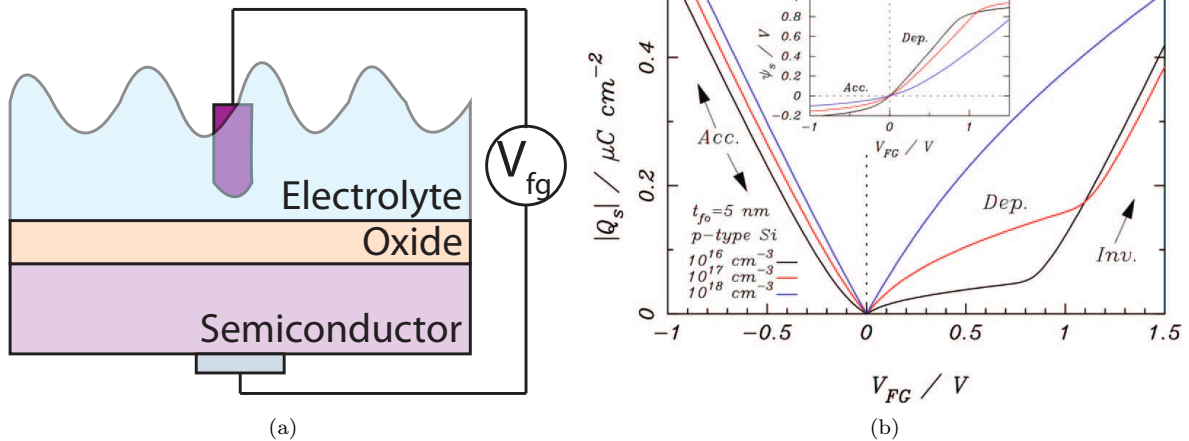


Figure 2.1: Electrolyte-oxide-semiconductor system. (a) Schematic overview of an EOS system. V_{fg} is the reference electrode voltage. (b) Silicon charge Q_s as function of V_{fg} in the accumulation (Acc.), depletion (Dep.) and inversion (Inv.) regions in p-type silicon with varying doping concentrations. Inset: surface potential ψ_{s} as function of V_{fg} [13].

is partially depleted and depends strongly on the silicon body doping. For larger V_{fg} an inversion layer is formed which is strongly dependent on the body doping concentration and thickness of the silicon body.

Considering ideal interfaces and ψ_0 equal to the potential drop across the reference electrode, the silicon is charge neutral (The (0,0) point in Figure 2.1b). When the reference electrode voltage biases the electrolyte, it creates a double layer on the oxide surface and an electric field perpendicular to the surface. The binding of H^+ to the surface can also create charge on the surface. Because of the conservation of charge, the charge on the oxide surface needs to be compensated in the silicon. If the reference voltage is decreased (left side of the plot), or pH of the electrolyte becomes more acidic, the charge on the oxide surface is also decreased. Due to charge conservation, positive charge from the semiconductor will start to accumulate on the semiconductor/oxide interface. This is the start of the accumulation region. If the voltage is positive, or when pH is more basic, for p-type silicon this means that first the area beneath the SiO_2 is depleted, because the mobile carriers will be repelled by positive charge on the surface, leaving negatively charged acceptor ions near the surface. When the voltage across the semiconductor is more than twice the bulk potential, an inversion layer of minority carriers (negatively charged for p-type) will form on the oxide/silicon interface, attracted to the positive charge on the surface. This layer is the inversion layer, the voltage at which this inversion layer starts is the threshold voltage.

2.3 The site binding model

The site binding model is used to model the equilibrium of protons between hydroxyl surface groups and hydrogen ions in a solution. It was first described by Yates et al. [14]. An interaction of the surface groups with the ions in solution originate a potential drop at the interface of electrolyte/insulator. The SBM in combination with the GCS model of the surface charge distribution can therefore be used to model the change in surface potential for a change in pH. The model described in this section was devised by Bousse et al. [2] and further extended by Van Hal et al. [4], who also looked into the differences with the Gouy-Chapman model.

Amphoteric surface sites can act as either donor or acceptor of protons. Commonly used oxides are SiO_2 and Al_2O_3 and an oxide surface site can be described with A-O^- , A-OH or A-OH_2^+ (Figure 2.2).

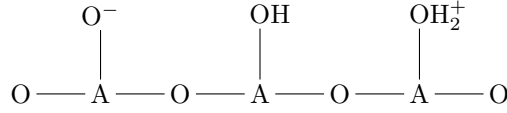
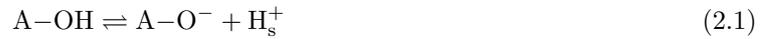


Figure 2.2: The amphoteric surface sites, from left to right the donor, neutral and acceptor sites.

For a neutral A-OH site, the acidic character can be given from reaction 2.1 [2] with the equilibrium constant K_a (2.2) [2, 4]. Acidic sites are proton donors.



$$K_a = \frac{[\text{A-O}^-][\text{H}^+]_s}{[\text{A-OH}]} = \frac{a_{\text{H}_s^+} \nu_{\text{A-O}^-}}{\nu_{\text{A-OH}}} \quad (2.2)$$

The basic character of this neutral site can be given from reaction 2.3 [2] with equilibrium constant K_b (2.4) [2, 4]. Basic sites are proton acceptors.



$$K_b = \frac{[\text{A-OH}_2^+]}{[\text{A-OH}][\text{H}^+]_s} = \frac{a_{\text{H}_s^+} \nu_{\text{A-OH}}}{\nu_{\text{A-OH}_2^+}} \quad (2.4)$$

In the equilibrium constants, $a_{\text{H}_s^+}$ is the activity of the protons in the direct vicinity of the oxide surface, via the Boltzmann equation (2.5) and the difference between the potential of the oxide surface and the bulk solution $\psi_0 = \psi_S - \psi_B$ [4]. ν_i represents the surface activity of a certain species i . The activity of protons is related to the pH via the Boltzmann equation, with pH_s the pH of the oxide surface and pH_B the pH of the bulk solution.

$$a_{\text{H}_s^+} = a_{\text{H}_B^+} e^{\frac{-q\psi_0}{kT}} \text{ or } pH_s = pH_B + \frac{q\psi_0}{2.3 kT} \quad (2.5)$$

The number of surface sites per unit area, N_s , is a fixed number [4] given by:

$$N_s = [\text{A-OH}] + [\text{A-O}^-] + [\text{A-OH}_2^+] \quad (2.6)$$

The surface charge density, σ_0 , depends on the number of charged surface sites [4] (Equation 2.7), in which q is the atomic charge and B is the number of basic groups:

$$\sigma_0 = q ([\text{A-OH}_2^+] - [\text{A-O}^-]) = -qB \quad (2.7)$$

2.3.1 Bousse model

Using Equations 2.6 and 2.7 one can set up a relation between pH, ψ_0 and σ_0 , yielding Equation 2.8 [2]:

$$[\text{H}^+] = \left(\frac{K_a}{K_b} \right)^{1/2} e^{y_0} \left(\frac{\left[\frac{\alpha_o}{\delta} + 1 + \left(\frac{\alpha_o}{\delta} \right)^{1/2} (1 - \delta^2) \right]^{1/2}}{1 - \alpha_o} \right) \quad (2.8)$$

where $y_0 = q\psi_0/kT$, $\alpha_o = \sigma_0/qN_s$ and the reactivity insulator surface $\delta = 2(K_a K_b)^{1/2}$. For oxides, this $\delta^2 \ll 1$.

In the case that $y_o = 0$ and $\alpha_o = 0$, so no surface potential or surface charge, the right hand portion of Equation 2.8 is 1, thus reducing it to Equation 2.9 [2]:

$$[H^+] = \left(\frac{K_a}{K_b} \right)^{1/2} \quad (2.9)$$

Equation 2.9 gives the H^+ concentration needed to have an electrically neutral surface, which is known as the point of zero charge (PZC), or pH_{pzc} .

The difference between pH and pH_{pzc} is given in Equation 2.10 [2]. This is used for Equation 2.11 [2], where the logarithm of Equation 2.8 is used with $1 - \delta^2 \approx 1$, as is the case for oxides. The first two terms are influenced by the number of surface sites A–OH and the last term is influenced by the saturation of the pH response if α_o nears 1.

$$v = \ln[H^+] - \ln \left(\frac{K_a}{K_b} \right)^{1/2} = 2.303 (pH_{pzc} - pH) \quad (2.10)$$

$$v = y_o + \sinh^{-1} \left(\frac{\alpha_o}{\delta} \right) - \ln(1 - \alpha_o) \quad (2.11)$$

In the case that the saturation term can be neglected, the following relation holds [2]:

$$v = y_o + \sinh^{-1} \left(\frac{y_o}{\beta} + \frac{\Delta\sigma}{qN_s\delta} \right) \quad (2.12)$$

In this formula, the dimensionless sensitivity parameter β is introduced, the ratio of voltage setup in the double layer by charge and thermal voltage [2].

$$\beta = \frac{q^2 N_s \delta}{C_{dif} k T} \quad (2.13)$$

For small values of the argument of the hyperbolic sine function, the sine will behave linearly and then the slope of function 2.12 is $\beta/(\beta + 1)$. Function 2.12 will then become [2]:

$$\psi_o = 2.303 \frac{kT}{q} \frac{\beta}{\beta + 1} (pH_{pzc} - pH) \quad (2.14)$$

This model is only valid for the linear region of the sine, which occurs in the range of potentials given by $|\psi_o \cdot q/kT| \ll \beta$. Also, for pH high above pH_{pzc} , oppositely charged counter ions will adsorb in the oxide surface. However, the effect of this phenomenon on the ψ_o, pH -relation is much smaller than on the σ_o, pH -relation.

2.3.2 Van Hal model

Combining equations 2.2, 2.4, 2.6 and 2.7, the following relation for the surface charge density as a function of the activity of the protons at the oxide surface, the equilibrium constants K_a and K_b and the number of surface sites N_s is found [15]:

$$\sigma_o = qN_s \left(\frac{a_{H_s^+}^2 - K_a K_b}{K_a K_b + K_b a_{H_s^+} + a_{H_s^+}^2} \right) \quad (2.15)$$

Small changes in $a_{H_s^+}$ (a change in pH_s) have an effect on the surface charge density, changing the number of basic groups B :

$$\frac{\partial \sigma_o}{\partial pH_s} = -q \frac{\partial B}{\partial pH_s} = -q \beta_{int} \quad (2.16)$$

The intrinsic buffer capacity β_{int} is represented by the change in the number of basic groups due to a change in surface pH, $\partial B/\partial pH_s$, it can buffer these small changes in the surface pH, pH_s , but not in the bulk pH, pH_B [4]:

$$\beta_{int} = N_s \frac{K_b a_{H_s^+}^2 + 4K_a K_b a_{H_s^+} + K_a K_b^2}{\left(K_a K_b + K_b a_{H_s^+} + a_{H_s^+}^2\right)^2} 2.3 a_{H_s^+} \quad (2.17)$$

Gouy-Chapman theory

Gouy and Chapman both thought of the diffuse layer to model the behaviour of an electrolyte/electrode interface. The charge on the solid surface is of equal value but of opposite sign as the charge in the solution. Ions in the solution therefore attract to the electrode interface, but thermal motion equalising the overall solution concentration counteracts this attraction. Equilibrium between these forces is given by the Boltzmann equation [4]:

$$c_i(x) = c_i^0 e^{\left(\frac{-z_i q \phi_x}{kT}\right)} \quad (2.18)$$

where ϕ_x is the potential at distance x with respect to the bulk solution, $c_i(x)$ and c_i^0 are molar concentrations of species i at distance x and the bulk respectively and z_i is the valence of ions. This equation can be used with the Poisson equation which relates charge density to potential to give an expression for the surface charge density in the diffuse layer [4]:

$$\sigma_{dl} = -\sqrt{8kT\epsilon_r\epsilon_0 n^0} \sinh\left(\frac{zq\psi_0}{2kT}\right) = -C_i \psi_0 = -\sigma_0 \quad (2.19)$$

This equation gives the following expression for the differential capacitance [4]:

$$C_{dif} = \sqrt{\frac{2z^2 q^2 \epsilon_r \epsilon_0 n^0}{kT}} \cosh\left(\frac{zq\psi_0}{2kT}\right) \quad (2.20)$$

In the Gouy-Chapman theory, ions are considered point charges that can approach a surface arbitrarily close. Near the surface, this causes unrealistic high ion concentrations for high values of ψ_0 . Therefore, Stern suggested an adjustment of the theory.

Gouy-Chapman-Stern-theory

The adjustment Stern proposed was a diffuse layer of charge starting at a distance x_H from the surface, which is the closest approach for the centres of the ions in the solution. The surface charge σ_0 is balanced by an equal and opposite charge in the electrolyte, σ_{dl} , the charge in the double layer (Figure 2.3). The opposite charges parallel to each other form the integral double layer capacitance $C_{dl,i}$. The potential difference over this capacitance is equal to ψ_0 , the difference between the potential of the oxide surface and the bulk solution. The charge in the diffuse layer, σ_{dl} , calculated using the Gouy-Chapman-Stern model, is given by [15]:

$$\sigma_{dl} = -\sqrt{8kT\epsilon_r\epsilon_0 n^0} \sinh\left(\frac{zq\psi_1}{2kT}\right) \quad (2.21)$$

In this equation, n^0 is the concentration of each ion in the bulk, the product of the concentration of the bulk, Avogadro's number and the volume: $n^0 = c_i \cdot N_A \cdot V$.

The diffuse layer starts at the end of the Stern layer, at x_H , the location of the Helmholtz plane. The potential at this point is ψ_H , given by Equation 2.22 [15], which is the difference between the surface potential ψ_0 and the potential over the capacitance of the Stern layer.

$$\psi_1 = \psi_0 - \frac{\sigma_0}{C_{Stern}} = \psi_0 - \frac{\sigma_0 x_H}{\epsilon_r \epsilon_0} \quad (2.22)$$

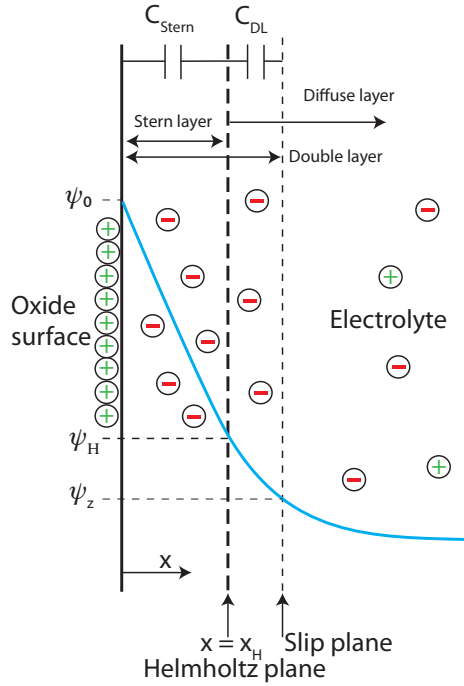


Figure 2.3: A schematic overview of the double layer at the oxide surface from the GCS model.

The differential double-layer capacitance C_{dif} is the ability of the double layer to store charge due to small changes in the potential $\partial\sigma_0/\partial\psi_0$, the slope of an $\sigma_0, \Delta\psi_0$ -plot. Its value is given by the following inverse formula [15], which is given in this form so that it is easy to see that the differential double layer capacitance is the sum of two capacitors in series, the Stern layer capacitance and the diffuse layer capacitance.

$$\frac{1}{C_{\text{dif}}} = \frac{\partial\psi_0}{\partial\sigma_0} = \frac{1}{C_{\text{Stern}}} + \frac{1}{\sqrt{\frac{2q^2 z^2 \epsilon_r \epsilon_0 n^0}{kT} \cosh\left(\frac{zq\psi_H}{2kT}\right)}} \quad (2.23)$$

With these formulas the effect of a small change in surface pH on the surface potential can be given [4]:

$$\frac{\partial\psi_0}{\partial\text{pH}_s} = \frac{\partial\psi_0}{\partial\sigma_0} \frac{\partial\sigma_0}{\partial\text{pH}_s} = \frac{-q\beta_{\text{int}}}{C_{\text{dif}}} \quad (2.24)$$

This can be written as the following formula of pH sensitivity of an oxide/solution interface, as found in ISFETs and SiNWs [4]:

$$\frac{\partial\psi_0}{\partial\text{pH}_B} = -2.3 \frac{kT}{q} \alpha \quad \text{with } \alpha = \frac{1}{\frac{2.3kTC_{\text{dif}}}{q^2\beta_{\text{int}}} + 1} \quad (2.25)$$

The α sensitivity parameter is dimensionless and varies between 0 and 1. It depends on the intrinsic buffer capacity β_{int} and the differential double-layer capacitance C_{dif} . The so-called Nernstian sensitivity of -59.2 mV/pH at 298 K occurs when $\alpha = 1$ and is therefore the maximum achievable sensitivity.

For theoretical curves of these models, refer to Chapter 4, Figures 4.1 - 4.3.

2.4 ISFET

The ion sensitive field effect transistor (ISFET) is a transistor that works in the same way as a metal oxide field effect transistor (MOSFET), without the metal gate but with a electrolyte solution and a reference electrode in its place. The reference electrode is placed to ensure a stable voltage in the electrolyte solution or to gate the device. The ISFET has three terminals: a source, a drain and a bulk. On top of these is an oxide layer (Figure 2.4).

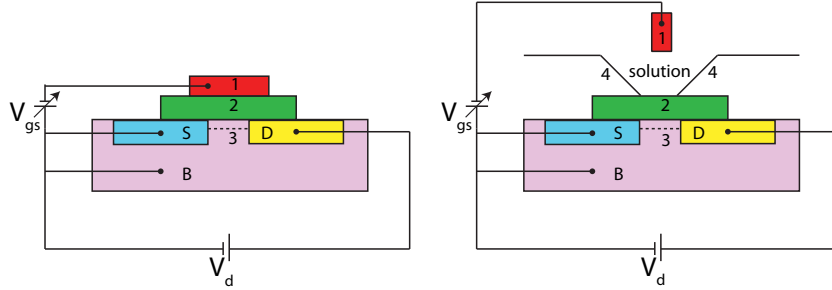


Figure 2.4: Schematic comparison between a MOSFET (left) and an ISFET (right). 1: reference, 2: gate oxide, 3: channel, 4: insulating resin, S: source, D: drain, B: bulk

From Section 2.2, this structure is known as an EOS system with SiO_2 as oxide and Si for the semiconductor. Charge on the oxide surface due to the electrolyte pH will deplete the region between source and drain, eventually creating an inversion region. The Nernst equation (2.26) gives the electrical potential difference at a solid/liquid interface such as the SiO_2 /electrolyte as a function of the ion concentration in the electrolyte and the activity coefficient: $a_i = f_i * c_i$ [15]. For dilute electrolytes, $f_i = 1$. The sensitivity factor depends on the gas constant R, the absolute temperature T and the Faraday constant F [15]:

$$E_I = \Delta\psi_0 = \frac{RT}{F} \ln \left(\frac{a_{i,1}}{a_{i,2}} \right) \quad (2.26)$$

If the drain voltage is higher than the gate-source voltage, the field created by the drain voltage will be larger than the field created by the gate voltage. This means that the channel will deform: it will increase in width at the source, but will be narrow near the drain. This effect is known as pinch-off. Below pinch-off, the drain current I_d for the non-saturated region, the region near the drain which is depleted, is given by [15]:

$$i_{ds} = \beta (V_{gs} - V_T - 1/2 V_{ds}) V_{ds} \quad (2.27)$$

with β a parameter determined by the mobility of the electrons in the inversion layer, the gate insulator capacitance and the width to length ratio of the channel and V_T the threshold voltage, the voltage at which the inversion layer is formed. The threshold voltage depends on the flatband voltage V_{fb} , the bulk potential of the silicon and the potential drop over the oxide.

Bousse et al. [2] state that for an EOS system, the voltage that is applied to a back contact which gives the silicon surface flat energy bands is known as the flatband voltage, Equation 2.28:

$$V_{fb} = E_{\text{ref}} - \frac{1}{q} \Phi^{Si} - \psi_o - \frac{Q_i}{C_i} + \chi^{\text{sol}} + \delta_\chi \quad (2.28)$$

The flatband voltage equation consists of several components:

- E_{ref} is the reference electrode potential, which for an ideal ISFET is the gate-source voltage V_{gs}
- $\frac{1}{q} \Phi^{Si}$ is the work function of silicon, approx. 4.7 V

- ψ_0 is the potential drop over the electrolyte/oxide interface, eq. 2.26
- Q_i is the effective charge per unit area in the insulator
- C_i is the insulator capacitance
- χ^{sol} is the surface dipole potential of the solution
- $\delta\chi$ is variations of χ potentials.

Three terms from the flatband voltage equation are influenced by the composition of the electrolyte used:

- ψ_0 , the potential drop in the electrolyte over the electrolyte/oxide interface
- $(d_c/d_i) \frac{Q_m}{C_i}$, mobile ionic charges which could be partly modulated by electrolyte presence, with Q_m charges distributed in the insulator
- Q_{it}/C_i , surface state densities which could be influenced by the electrolyte, because of diffusion through the insulator of some species.

2.4.1 Previous work on ISFETs

Bousse et al. [2] revised the site binding model of Yates [14] for ISFETs and tested the theory using a electrolyte/SiO₂/silicon capacitor. The SiO₂ surface was exposed to the background electrolyte at pH_{pzc} for a couple of hours before measurements. Shifts in flatband voltage V_{fb} were measured while pH was increased in steps of 0.3 or 0.4 points until pH = 5. In the Bousse model, the β -parameter was the slope of the pH, ψ_0 -curve, and the best fit of theory to experimental results was with $\beta = 0.14$. This corresponded with a ΔpK of 6.9, $N_s = 5 \cdot 10^{14} \text{ cm}^{-2}$ and $C_{\text{stern}} = 20 \text{ }\mu\text{Fcm}^{-2}$. The model was found to be correct in a region of 2.5 pH-points around pH_{pzc} .

Van Hal et al. [4] further expanded the Bousse model so that it could be used for pH up to 10. The sensitivity of ISFETs with SiO₂ gate material was found to be 45 mV/pH in the neutral area (pH > pH_{pzc}) while it was remarkably lower at pH_{pzc} , which results in an α between 0 and 0.75.

2.4.2 Effect of monolayers

Van den Berg has researched the effects of different equilibrium constants K_a and K_b on the sensitivity of an ISFET [3] by adding a monolayer of a material with a higher or lower pK_a or pK_b than SiO₂ and measuring the resulting ψ_0, pH_B -response. It was found that increasing or decreasing pK_a values shifted the point of zero charge pH_{pzc} (net amount of surface charge is zero) of non-Nernstian surfaces 1.5 pH point upwards or downwards respectively. Nernstian surfaces had a linear pH-curve with a slope of 55 - 60 mV/pH. Increasing or decreasing pK_b values shifted the pH response above pH_{pzc} 3 pH points towards lower or higher pH values respectively.

The number of surface sites, N_s also influenced the ψ_0, pH_B -graph. An increase in N_s gave the pH response a higher slope, while lower N_s results in a lower slope.

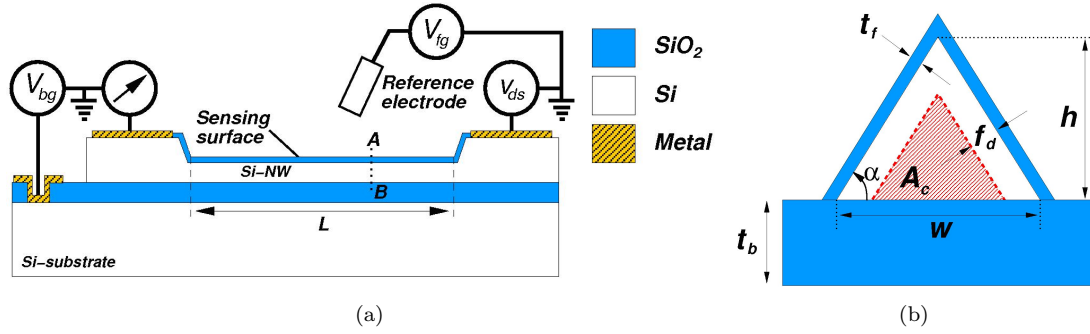


Figure 2.5: Cross-sectional views of silicon nanowire [6]. (a) Lengthwise cross-section, with cross-section of (b) indicated with A-B. (b) A-B cross-section

2.5 Silicon nanowires

Masood et al. [6] have made an electrical model of the triangular SiNWs. The conductance in the channel, G_c , is defined as the change in the drain current, i_{ds} , for a change in the drain-source voltage V_{ds} : $G_c = \partial i_{ds} / \partial V_{ds} = \mu_b Q_c L^{-1}$ [6]. It depends on the mobility of the majority carriers μ_b , the length of the nanowire L and the majority carrier charge per unit length Q_c . From this we can find the drain source current:

$$i_{ds} = V_{ds} G_c = V_{ds} \frac{\mu_b Q_c}{L} \quad (2.29)$$

This device can also be modeled as an EOS system. But the nanowire is three dimensional, so the two sides of the triangle are two EOS systems that interact. A change in surface potential $\Delta\psi_0$ results in a change in channel conductance because of a field effect across the dielectric layer. This field effect is in a cross-sectional area A_c (Figure 2.5a), such that the channel conductance is modulated $G_c \pm \Delta G_c$ as the channel charge is $Q_c = q N_a A_c$ with N_a the doping concentration, assumed to be uniformly distributed in the nanowire.

The cross-sectional area A_c (see figure 2.5b) as function of the surface potential can be modeled as [6]:

$$A_c(f_d) = 1/2 \left(w - \frac{2f_d}{\sin\alpha} \right) \left(h - \frac{f_d}{\cos\alpha} \right) \quad (2.30)$$

in which w is the width of the wire, h the height, α the base angle and f_d the depletion function [6]:

$$f_d = \sqrt{\left(\frac{\epsilon_{si}}{\epsilon_{ox} t_f} \right)^2 + 2\epsilon_{si}\epsilon_o \frac{(V_{fg} - V_{fb})}{qN_a}} - \frac{\epsilon_{si}}{\epsilon_{ox} t_f} \quad (2.31)$$

The frontgate voltage V_{fg} is used to set the operation point of the sensor and V_{fb} is the flatband voltage (Equation 2.28). It is assumed that the frontgate voltage compensates the various potential drops completely such that $V_{fg} - V_{fb} \approx \psi_0$.

2.5.1 Previous pH-measurements on SiNWs

Knopfmacher et al. [8] researched the pH sensitivity of a dual-gated silicon nanowire (top down fabrication) and found that it was above the Nernst limit of 60 mV/pH. The results were reproducible and were founded on leakage- and hysteresis-free operation of the nanowires. The pH-induced backgate voltage shift can be enhanced if the capacitance over the backgate is smaller than the capacitance over the liquid-gate, the capacitances of the double layer and the oxide in series. For bottom up fabricated SiNWs, a sensitivity

of 58.3 mV/pH was reported by Hsu et al. [7], using the Bousse model, close to the Nernstian maximum. Elström et al. [16] researched the size dependence of the surface charge sensitivity for SiNWs. The SiNWs used were fabricated top down with varying width and a length of 10 μm . After oxidation, an APTES layer was applied. They found that the threshold voltage decreased if the nanowire width increased, this was reflected in an increased sensitivity for surface charges for smaller widths. Smaller nanowires had large conductance changes, while larger wires remained unaffected. The model used for these calculations was the Van Hal GCS model. Nikolaides et al. [17] used the Bousse model for their measurements on silicon nanowires. The results showed a β -parameter of 0.15, close to the one found by Bousse, which was 0.14.

2.6 Comparison ISFETs and SiNWs

Besides the scale difference, ISFETs are μm -scale and SiNWs are nm-scale, the interfaces are similar, with the exception that most ISFET silicon surfaces are oriented on the $\langle 100 \rangle$ plane, while the SiNWs we use have $\langle 111 \rangle$ plane orientation. The ISFET (Figure 2.4, right) has a bulk with two wells of differently doped material than that bulk, serving as source and drain for the electrical carriers which create a channel. This channel is formed due to the field effect created by the binding of protons from a solution to the surface sites of the oxide layer or by applying a voltage to the reference electrode. The field effect depletes the area between source and drain and brings minorities from the bulk to the surface. From the EOS-system point of view, the ISFET works in the depletion/inversion regime.

The nanowire (Figure 2.5a) has no bulk, but does have two wells (the place where the electrical connections are made) where there are more electrical carriers than in the wire itself, such that these pads serve as source and drain and the wire serves as a channel. It also has a second layer of silicon beneath a boxed oxide layer serving as a second gate. The wire, which is depleted through gating, is three dimensional (see Figure 2.5b) instead of the two dimensional depletion layer which forms the channel in an ISFET. The depletion layer is formed due to the field effect created by the same factors as the ISFET, but there is a third option, the backgate silicon, where another field effect could influence the wire. Therefore, the depletion layer has three surfaces from which it originates: the top oxide has two surfaces and the boxed oxide.

Chapter 3

Experimental

3.1 Introduction

In this Chapter, all the necessary information for the experiments done in order to find an answer to the research questions is found. The goal of the experiments is to acquire data to test the Van Hal site binding model as described in Section 2.3 for the triangular SiNWs from Section 3.3. To do this, SiNWs are subjected to a solution with varying pH while the frontgate voltage is scanned.

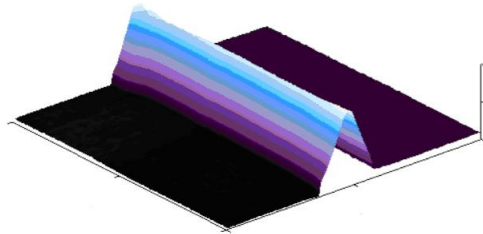
3.2 The reference electrode

For the experiments done for this thesis, a reference electrode will be used. The importance of a reference electrode was made clear in an article by Minot et al. [18], who did their research on carbon nanotubes, which are comparable in signal strength to SiNWs. Platinum and silver/silverchloride electrodes were compared. In a buffer solution where reduction/oxidation species are not controlled, biomolecule binding sensors are operated. Background redox reactions are slow. The interface voltage is unstable and unpredictable in this situation. With a Ag/AgCl reference electrode the metal-solution interface is separated from the analyte solution with a frit, which blocks large molecules from reaching the metal surface. In this manner, the reduction/oxidation conditions are controlled. The Pt electrode has a 300 mV lower solution potential than the Ag/AgCl electrode, due to different metal-liquid interfaces and surface electrochemistries.

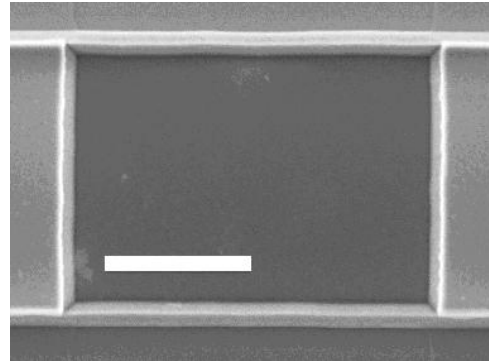
3.3 Silicon nanowire device structure

There are two ways of fabricating SiNWs. The first technique is bottom-up fabrication where the device is assembled from an atomic level through Vapour Liquid Solid growth method. A metal droplet (usually Au) is used to create homogeneous nuclei of a semiconductor. These aggregate cluster blocks are seeds for further growth and form larger structures. The diameter of the wire is defined by the diameter of the metal droplet and the furnace conditions. Doping can be done by adding dopants to the precursor gas. Problems with this technique are the formation of ohmic contacts, as electrodes are not easily attached to the wires, and the lack of controlled growth into high density arrays, which makes high volume production difficult.

Top down fabrication, used by the BIOS group and used for chips for this thesis, is based on standard microfabrication techniques [5]. A thin silicon nitride (SiN) layer is patterned on a silicon-on-insulator wafer as a mask for plane-dependent wet etching (PDE) on the (110)-plane. After etching, the exposed



(a) Tapping mode atomic force microscope (AFM) image of a SiNW, nanowire height is 90 nm.



(b) High-resolution scanning electron microscopy (HRSEM) image of triangular SiNWs (scale bar: 1 μm)

Figure 3.1: Microscope images of SiNWs

(111)-sides are thermally oxidised. Another lithography step patterns and etches the SiN mask layer for a second time, with another PDE step creating triangular cross section SiNWs. In the final step, metal contacts and gate oxide are applied. For further information, see the paper of Chen et al. [5].

The resulting nanowires from this fabrication process are triangular, as can be seen in Figure 3.1.

3.4 Methods

3.4.1 Packaging

Chips with the SiNWs are tested on the microscope stage with measurements done in air. When at least one nanowire in the range 10 - 50 μm is working, chips are glued to an ISFET board and wirebonded to the boards contacts. Hysol is used as a cover material, with the space above the nanowires left uncovered. It is important to cover all edges of the chip as these would short the wire when in contact with buffer solution. The hysolated chip needs to set in the oven for 3 hours. Before each measurement, the chip is cleaned in ozone plasma for 2 to 5 minutes, depending on when the last cleaning has taken place.

3.4.2 Monolayers

To change the number of surface sites, the nanowires were not only measured with bare SiO_2 but also with an added monolayer of either 3-aminopropyltriethoxysilane (APTES) or hexamethyldisilazane (HMDS).

The APTES monolayer is applied by submerging the packaged chip in a 1% APTES in ethanol solution for 30 minutes. After rinsing three times with ethanol, the chip is left to dry for five minutes in an oven at 120 $^\circ\text{C}$. APTES will form a layer of amine (NH_2) sites (see Figure 3.2a), a base with $pK_a \approx 9$ [5]. Below $pH = 9$, these groups are positively charged, increasing the depletion layer width and reducing i_{ds} . Another value for pK_a was found in the paper of Vezenov et al. [19], where it was found to be approximately 4. This value was found for single atom monolayers. This would mean that the monolayer would be positively charged below $pH = 4$.

For HMDS monolayers, the chip is dipped in HMDS and left in a closed container in an oven at 80 $^\circ\text{C}$ for an hour. HMDS will form a layer of CH_3^+ sites, nonpolar methyl groups which do not react with hydroxyl groups in pH range 2-10. Therefore, the sites where HMDS has bonded to the oxide will now

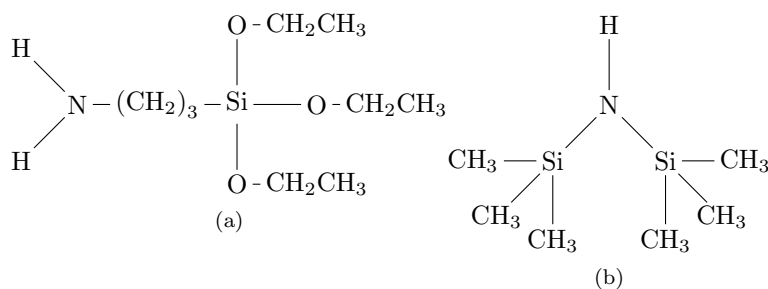


Figure 3.2: The molecular structure of the monolayers. (a) APTES (B) HMDS

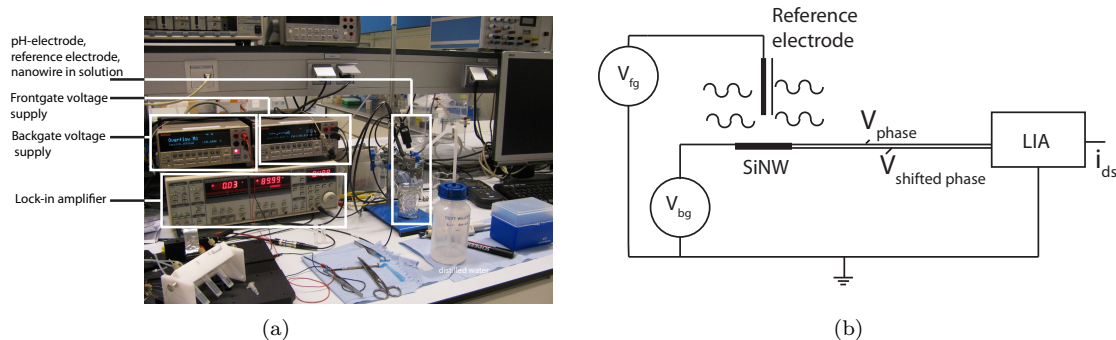


Figure 3.3: Photograph and schematic of the experimental setup

no longer contribute to the number of surface sites, effectively lowering N_s and the pH sensitivity of the device.

3.4.3 Electrochemical measurements

A buffer solution, consisting of 0.01 M universal buffer mixture (0.1 M citric acid, 0.1 M phosphoric acid and 0.2 M boric acid) and 0.1 M NaCl, $\text{pH} \approx 2.6$, is titrated to $\text{pH}_{pzc} = 2.1 \pm 0.04$ using 0.1 M HCl. The chip rests in this solution for 2 hours to equilibrate. A calibration curve is recorded by measuring the drain-source current i_{ds} on a lock-in amplifier (LIA, SR830, Stanford Research Systems) as a function of the frontgate voltage V_{fg} (Keithley 2400) in steps of 0.1 or 0.05 V, depending on the range of interest. For the LIA, the reference signal was set to 500 mV, 30 Hz modulation frequency. The backgate voltage V_{bg} (Keithley 2400) is either grounded or set to a fixed voltage. From this data, a V_{fg} is chosen with high sensitivity (the point where the slope of the V_{fg}, i_{ds} -graph is high and linear). Using this fixed V_{fg} a series of measurements is done with varying pH of the solution, in steps of 1 pH-point, until $\text{pH} = 10$. This is done by titrating the solution with 0.1 M NaOH. Using this data, the change in surface charge per pH can be calculated using the earlier acquired V_{fg}, i_{ds} -graph. The reference electrode used for the measurements is an Ag/AgCl reference electrode (Radiometer analytical). A photo of the set-up, with the lock-in amplifier beneath the voltage sources for front- and backgate, is seen in Figure 3.3(a), along with the measurement schematic (b). For some measurements a dedicated Labview program, developed by Dirk-Jan van den Broek, was used, which automated the frontgate and pH sweep measurements. This program had no influence on the nanowires as all interaction was through the measurement appliances. It could set front- and backgate voltages, measure these voltages, the drain-source current and pH.

3.5 Comparison ISFET method and SiNW method

For ISFETs at a fixed drain-source voltage, the changes in gate potential can be compensated for by a modulation of the gate-source voltage. A special ISFET amplifier uses negative feedback to keep the drain current constant, so that the change in V_{gs} can be measured, see Figure 3.4.

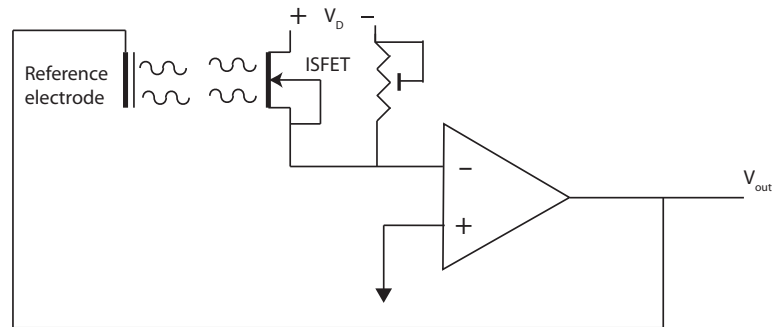


Figure 3.4: A schematic circuit overview of a negative feedback loop to keep i_{ds} constant, as found in an ISFET amplifier

However, the ISFET amplifier needs a certain amount of i_{ds} to function properly ($i_{ds} > 1\mu A$). As i_{ds} for SiNWs is too low, a lock-in amplifier (LIA) is used. A lock-in amplifier consists of a mixer followed by a low pass filter (Figure 3.5). It compares the incoming sine wave signal to a reference sine wave and generates the sum and difference frequencies in the mixer. The low pass filter then filters out everything but the difference frequencies below a certain cut-off frequency. This output, which also depends on the relative phases of the incoming and reference signals, has the same spectral information as the original signal but in a narrow band around the reference frequency. Adjusting the cut-off and reference frequency allow for signals of arbitrary bandwidth to be measured.

The main advantage of using a lock-in amplifier is the increased signal to noise ratio, as the amount of noise is proportional to the bandwidth. The LIA sends a sine wave through the SiNW, which is then

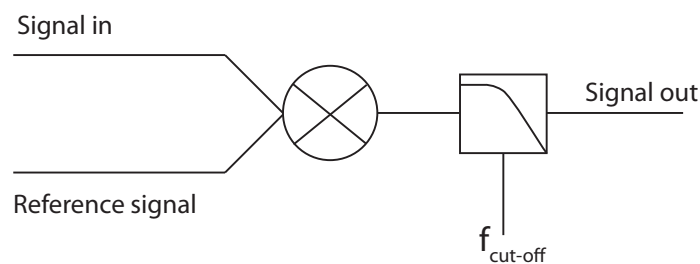


Figure 3.5: A schematic overview of a lock-in amplifier

compared to the reference sine wave generated by the LIA itself. Through this, the drain current in the nanowire can be measured, which is in the nanoampère range. A V_{fg}, i_{ds} -graph can be made and the derivative of this graph is used to get the sensitivity of the chip. From an i_{ds}, V_{fg} -graph, the change in surface potential can be found by finding a fit for the measurement points around the voltage which resulted in the highest sensitivity. Using this formula, the change in surface potential can be found after changing pH and measuring the difference in generated i_{ds} . The ISFET method measures the surface potential directly, while with the SiNW method a lot more calculations are needed.

Chapter 4

Results and discussion

4.1 Introduction

The Results Chapter gives an overview of all the measurements done in order to answer the research questions, as well as what they mean and how the theory can be applied to them.

4.2 Theoretical curves

The following curves were plotted using Mathematica files as found in Appendix A. The first curve, Figure 4.1, shows the pH, ψ_0 -curve of the Bousse model (Section 2.3.1), with a varying β parameter. The slope is influenced by this parameter, as indicated by the results of experimental work of Bousse [2] and Van den Berg [3] (Section 2.4.1). However, the experimental work of Bousse et al. also implied that this model was only accurate in the pH range 1.0 - 4.7. The curves show that the β parameter, which depends on the number of surface sites and the differential double layer capacitance, influences the slope of the curve in this pH range: a higher β gives a higher slope, eventually making the graph linear. Above this range, the slope is the same for all curves.

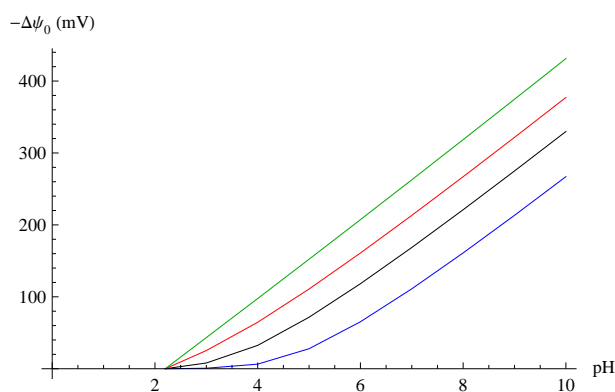


Figure 4.1: Theoretical total response of a SiO_2 ISFET, according to the Bousse model. The different coloured lines have different β . Blue: 0.01; black: 0.14; red: 1; green: 10. $\beta=0.14$ gave the best fit to the measurement results of Bousse.

The Van Hal model using the Gouy-Chapman theory (GC-theory, Section 2.3.2) results in the graphs of Figure 4.2. The concentration of the electrolyte has been varied in Figure 4.2a, as the electrolyte

concentration influences the Stern layer, which is not accounted for in the GC-theory. In Figure 4.2b, the results of Van den Berg (Section 2.4.2) can be confirmed theoretically. When the number of surface sites increases, so does the slope of the pH, ψ_0 -graph. However, because the GC-theory sees charges as a point charge, an infinite amount of charges can accumulate on the surface, which in practice is impossible. The model will go into imaginary numbers for high pH, at which pH this starts depends on the number of surface sites. As can be seen, the graph for $N_s = 5 \cdot 10^{17}$ ends at little over $pH = 8.3$.

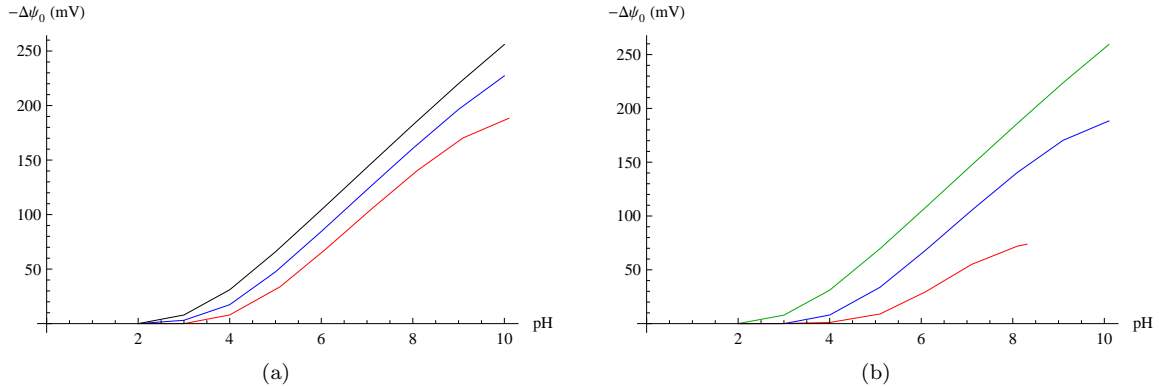


Figure 4.2: Theoretical total response of a SiO_2 ISFET, according to the Van Hal model using the Gouy-Chapman theory. $C_{i,st} = 0.8 F/m^2$ (a) The different coloured lines have a different molar concentration of the electrolyte, c_o . Black: 1 mM; blue: 0.01 M; red: 0.1 M. (b) The different coloured lines have a different number of surface sites, $c_o = 0.1M$. Red: $5 \cdot 10^{17}$; blue: $5 \cdot 10^{18}$; green: $5 \cdot 10^{19}$

Using the Gouy-Chapman-Stern theory (Section 2.3.2), which uses the added Stern capacitance to compensate for the size of charges, the graphs of Figure 4.3 are obtained. Here, in Figure 4.3a, the concentration of the electrolyte is varied in the same way as with the GC-theory. However, in these graphs, it is shown that for higher pH, the concentration does not have as high an influence as with the GC-theory. In Figure 4.3b the influence of the number of surface sites is shown. As this model has no restrictions due to the sinh-function and uses the Stern capacitance, which improves the GC-theory, the parameters of the measurements will be extracted using this model.

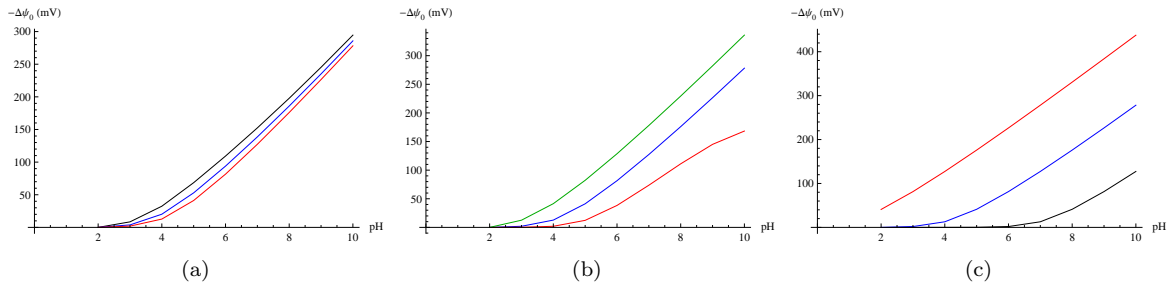


Figure 4.3: Theoretical total response of a SiO_2 ISFET, according to the Van Hal model using the Gouy-Chapman-Stern theory. $C_{i,st} = 0.8F/m^2$. (a) The different coloured lines have a different molar concentration of the electrolyte, c_o . Black: 1 mM; red: 0.01 M; blue: 0.1 M. (b) The different coloured lines have a different number of surface sites N_s . $c_o = 0.1 M$. Red: $5 \cdot 10^{17}$; blue: $5 \cdot 10^{18}$; green: $5 \cdot 10^{19}$. (c) Influence of K_a value on the pH, ψ_0 -plot. Black: $pK_a = 3$; blue: $pK_a = 6$; red: $pK_a = 9$

In Figure 4.3c, a graph can be seen representing the experimental results of Van den Berg et al. [3] (Section 2.4.1), showing the results of varying the K_a -value. The increase of K_a results in a shift of the graph in the basic direction, the decrease of K_a results in a shift in the acidic direction. As the pK_a -values are a negative logarithm, an increase of K_a corresponds with a decrease of pK_a .

4.3 Electrical measurements

The electrical measurements were frontgate sweeps of a chip in solution prepared according to the directives in Section 3.4.3. As mentioned in that Section, the sweep was done at either zero or at a constant backgate voltage, whichever gave satisfactory response ($\Delta i_{ds} \geq 60$ nA over the whole sweep). The measurements were done before all pH measurements, in order to determine the best sensitivity from the derivative of this graph. At the point where the derivative is zero, the sensitivity is highest. Figure 4.4 shows an example of the results of two sweeps, with the $\partial i_{ds} / \partial V_{fg}$ -graph below. T

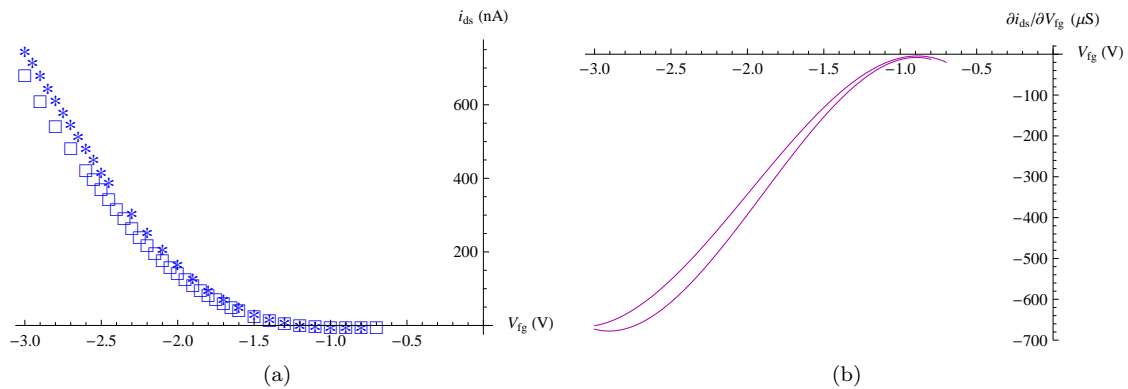


Figure 4.4: (a) Frontgate sweep of a silicon nanowire, 20 μ m length. Buffer: 0.01UBM with 0.1M NaCl. (b) $\partial i_{ds} / \partial V_{fg}$ -graph of (a)

4.4 pH measurements on bare SiO_2

The pH measurements as described in Section 3.4.3 were done after the electrical measurements. The surface potential can be calculated using the i_{ds}, V_{fg} -graph of the electrical measurements and finding the trend line for the results around the voltage which gives the highest sensitivity. The voltage at which this highest sensitivity is found is used for these measurements. The change in drain current due to the change in pH of the solution is used to calculate the difference in ψ_0 , using the trendline found from the electrical measurements. The ψ_0, pH -plot is found in Figure 4.5. The graph shows the same shape as the Bousse and Van Hal model curves from the previous Section (Figures 4.1 - 4.3). The slope of the measurements is at 47.7 mV/pH lower than values found in literature 2.5.1.

4.5 Monolayer pH measurements

4.5.1 APTES functionalisation

The pH measurements of wires with a monolayer of APTES, applied according to the directives in Section 3.4.2. The measurements were done in the same manner as the bare SiO_2 nanowire measurements, with

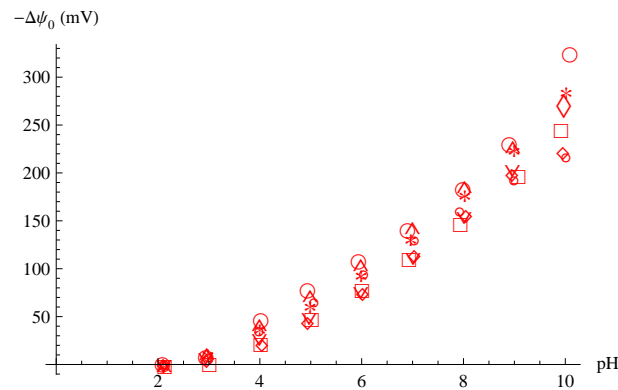


Figure 4.5: pH measurements on 10 μm and 20 μm long bare SiO_2 nanowires. Buffer: 0.01UBM with 0.1M NaCl. Frontgate voltage set to value with highest selectivity. Each icon represents one measurement series, 7 total: *, \square , \diamond : 10 μm ; \circ , \wedge , \square , ∇ : 20 μm . Slope: 47.7 mV/pH at pH = 8.

a frontgate sweep to acquire the most sensitive spot. The $pH, \Delta\psi_0$ -curve shows an increased slope in comparison to the bare SiO_2 nanowires. The curves of figure 4.3b indicate that the number of surface sites influences the slope of the $pH, \Delta\psi_0$ -curve. As mentioned in Section 3.4.2, APTES has a pK_a of approximately 9, which is higher than the pK_a of SiO_2 which is approximately 6 [2]. The expected shift to the acidic site has occurred, giving the whole pH range an equally high sensitivity.

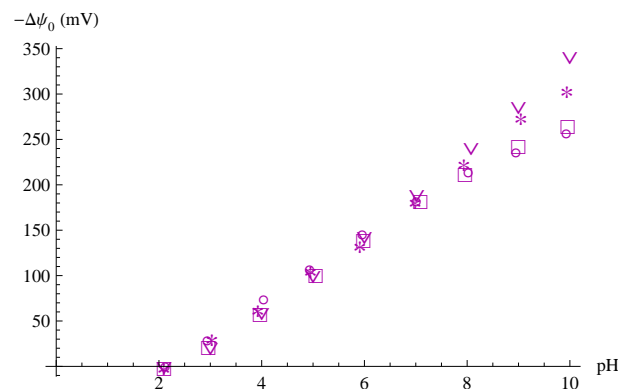


Figure 4.6: pH measurements on APTES functionalised nanowires. Buffer: 0.01UBM with 0.1M NaCl. Each icon (\square , *, ∇ , \circ) represents one measurement series, 4 total. Slope: 38.19 mV/pH in whole pH range.

4.5.2 HMDS functionalisation

The pH measurements of wires with a monolayer of HMDS, applied according to the directives in Section 3.4.2. This $pH, \Delta\psi_0$ -curve shows a decreased response to the pH change in comparison to the bare SiO_2 nanowires. This is consistent with the expectation of the HMDS decreasing the number of surface sites (refer to Section 3.4.2), thus decreasing the slope, like the theory in graphs reffig:GCNsdif,fig:GCSNsdif suggested.

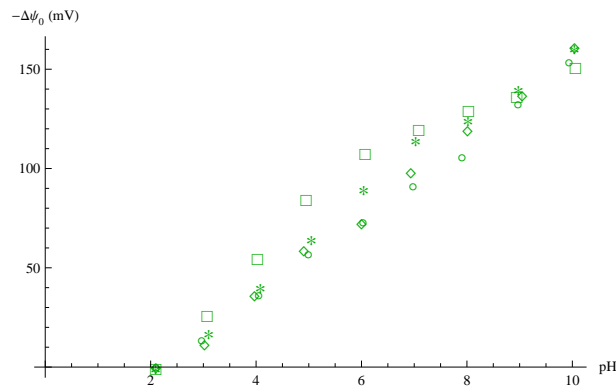


Figure 4.7: pH measurements on HMDS functionalised nanowires. Buffer: 0.01UBM with 0.1M NaCl. Each icon ($\square, \diamond, *, \circ$) represents one measurement series, 4 total. Slope: 17.06 mV/pH at pH=9.

4.6 Parameter extraction

As mentioned in Section 2.6, the silicon plane orientation of SiNWs and ISFETs differs. From literature, N_s of $\langle 100 \rangle$ -plane pure silicon (used in ISFETs) is $6.8 \cdot 10^{18}$ atoms/m². This number has been corrected for the SiO₂ surface to $N_s = 5 \cdot 10^{18}$ [20]. However, for $\langle 111 \rangle$ -plane pure silicon this number is $7.85 \cdot 10^{18}$ atoms/m² [21]. It is therefore interesting to see if the NW pH behaviour reveals larger N_s values than found for ISFETs. The fitting of the measurement results with the theoretical models will therefore be dependent on N_s .

The measurement results are plotted together with the graphs of Figure 4.3b of the Van Hal model using GCS theory. This results in the graph of Figure 4.8a. From this graph, a rough estimate of N_s can be given: the curve for $N_s = 5 \cdot 10^{18}$ is very close to the average measurement curve. This figure

A relative χ^2 -test was used to determine the best fit for the measurement data. The χ^2 test uses the following formula [22]:

$$\chi^2 = \sum_{i=1}^n \frac{(\psi_{0m_i} - \psi_{0c_i})^2}{\psi_{0c_i}} \quad (4.1)$$

where the index m indicates a measurement result and c a theoretical result. The best fit is for the theoretical result that results in the lowest χ^2 function.

Various values for N_s were used, starting with the values from literature $N_s = 5 \cdot 10^{18}$ and $7.85 \cdot 10^{18}$ atoms/m², along with other values in the same order of magnitude. A graph of these values was made, then new values for N_s were chosen based on this graph, in order to end up with a minimal χ^2 value. The best fit was found for $N_s = 1.5 \cdot 10^{19}$ atoms/m² (Figure 4.8b). This indicates that the SiNW $\langle 111 \rangle$ -surface has an increase in N_s over the ISFET $\langle 100 \rangle$ -plane. Other influences on the slope could be the value chosen for the Stern capacitance, the electrolyte concentration or the

Because a lot of literature uses the Bousse model for SiNWs, a fit for this model is also presented in figure 4.9b. As the model is only valid for a part of our measurement range, only the valid range has been taken into account. This results in a β -parameter of 0.15, only slightly higher than the parameter found for ISFETs (0.14). However, the number of measurement points is rather low, as the pH was only changed in steps of 1 pH -point, and this graph might not give good result for the fit. The higher β value indicates that either N_s or the differential double layer capacitance is different for SiNWs in comparison to ISFETs. Again, a valid explanation could be that the $\langle 111 \rangle$ -surface has a higher number of surface sites. Other groups have found β to be 0.15 [17] or 0.22 [5].

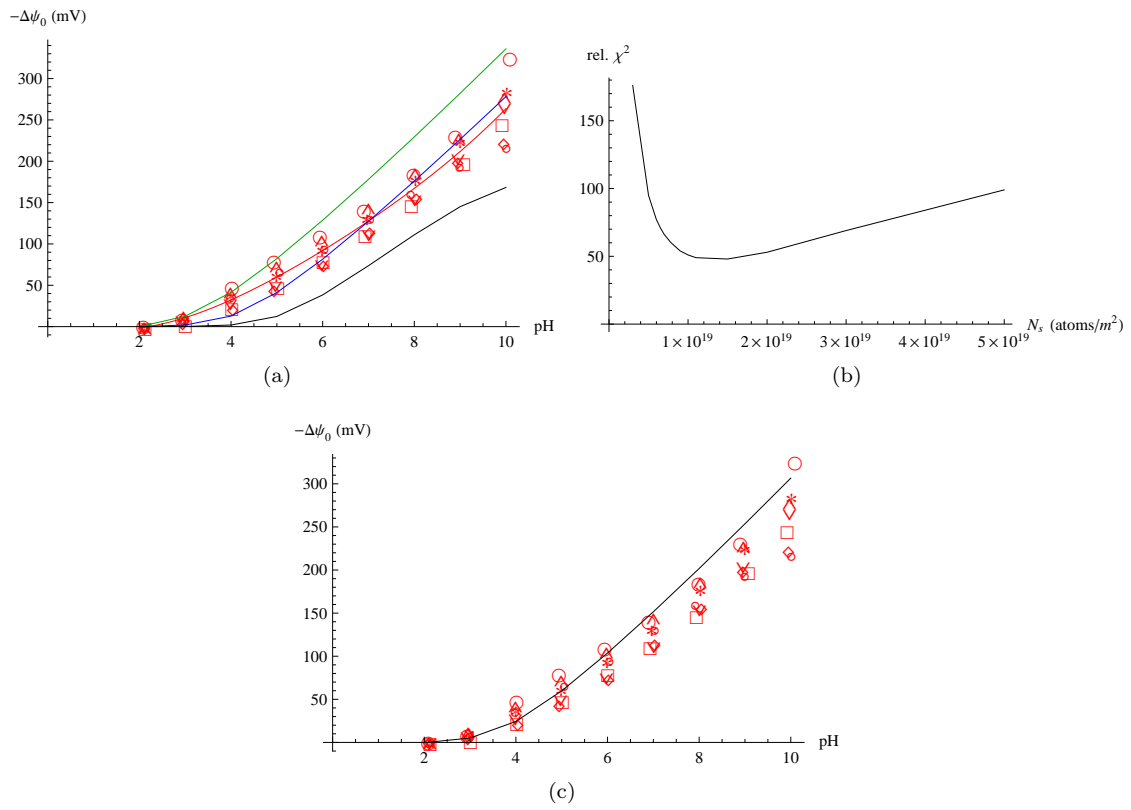


Figure 4.8: Measurement results (red markers) and their theoretical fit. (a) The black, red and green line are GCS-theory Van Hal model curves with different N_s , black $5 \cdot 10^{17}$ atoms/m², blue $5 \cdot 10^{18}$ atoms/m², green $5 \cdot 10^{19}$ atoms/m². (b) χ^2 values for different values of N_s . (c) The black line indicates the fit of the GCS-theory Van Hal model with best fit $N_s = 1.5 \cdot 10^{19}$ atoms/m². $c_o = 0.1$ M, $C_{i,st} = 0.8F/m^2$

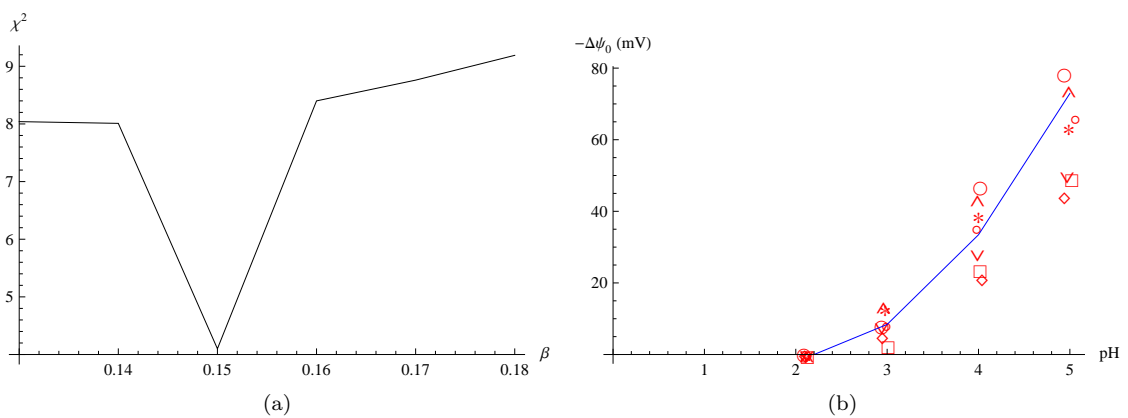


Figure 4.9: (a) χ^2 values for varying values of β . Best fit for $\beta = 0.15$. (b) The blue line indicates Bousse model fit with $\beta = 0.15$.

Chapter 5

Conclusion

In the Introduction, the following research questions were formulated, which will be answered in this Chapter:

- How do silicon nanowires compare to ISFETs?
- What is the behaviour of silicon nanowires in changing pH solution?
- Are the extended parameters that characterise the surface the same for ISFETs and SiNWs? If not, why?

Three models exist for the ISFET. The Bousse model (Figure 4.1) uses an approximation which makes the model only valid for a small pH -range ($pH = 1.0 - 4.7$). The Van Hal model has two versions, one incorporating the GC theory and one incorporating the GCS theory. The graphs of the Van Hal model, shown in Figure 4.2 and fig:theoryGCSgraphs, underline the fact that the GC theory can be used as a fast approximation, but for more detailed work, the GCS theory should be used.

SiNWs are by definition an EOS system. Unlike the ISFET, the SiNW is a majority carrier device with a three-dimensional channel, which can be gated using the top oxide layer or the boxed oxide layer beneath the device through the back gate. The surface of SiNWs is $\langle 111 \rangle$ -plane silicon, whereas ISFETs are usually $\langle 100 \rangle$ -plane. The drain current i_{ds} is also several orders of magnitude smaller than the ISFET, nA versus μA . Results show that the top-down fabricated, p-type triangular SiNWs as used by the BIOS group act as an EOS FET (Figure 4.4). This is an answer to the first research question.

Furthermore, the experiments show that the surface charge of silicon nanowires changes with pH (Figure 4.5). Functionalisation of the surface with materials that changed pK_a (APTES) or blocked surface sites (HMDS) of the SiO_2 on top of the nanowire has shown that the pH sensitivity can be changed. These results answer the second research question.

The results correspond with the theory that ISFETs and silicon nanowires can be described using the same models, which are based on the EOS system and the SBM. However, due to the geometrical differences, some parameters should not be taken blindly from the ISFET model. The triangular shape results not only in a three dimensional channel, but also in two $\langle 111 \rangle$ -plane silicon surfaces, which according to literature have a higher number of surface sites. The Van Hal model fit to experiment results confirms this (Figure 4.8c). The number found for SiNWs, $N_s = 1.5 \cdot 10^{19}$, is three times higher as that for ISFETs, $N_s = 5 \cdot 10^{18}$. However, using the Bousse model, a parameter not unlike that for the ISFETs was found, $\beta = 0.15$ for SiNWs and $\beta = 0.14$ for ISFETs (Figure 4.9). The Bousse model is however only valid on a limited pH -range in which only 4 measurement points were taken for each experiment, so this value might not be very accurate. This answers the third research question.

Appendix A

Mathematica files

A.1 Bousse model

```

Clear[A, B, \[Psi]s];
pHpzc = 2.2; (*they took pHpzc to be 2.2, see graph with beta=0.14*)
pH = {2.2, 3, 4, 5, 6, 7, 8, 9, 10};
q = 1.6*10^-19;
k = 8.61734315*10^-5;
T = 300;
A = 2.303*(pHpzc - pH);
\[Beta] = 10;
B = \[Psi]s/(k*T) + ArcSinh[\[Psi]s/(k*T)*1/\[Beta]];
For[i = 1, i < 10, i++,
  Print[FindRoot[A[[i]] - B == 0, {\[Psi]s, 0}]]]
  datanul = { {0, 0}};
dataSBMBousse014 = {{2.2, 0}, {3, 7.99}, {4, 32.46}, {5, 71.60}, {6,
  118.19}, {7, 168.56}, {8, 221.08}, {9, 274.98}, {10,
  329.82}}; (*beta=0.14*)
dataSBMBousse001 = {{2.2, 0}, {3, 0.7}, {4, 6.38}, {5, 27.83}, {6,
  65.31}, {7, 111.11}, {8, 161.05}, {9, 213.32}, {10,
  267.05}}; (*beta=0.01*)
dataSBMBousse1 = {{2.2, 0}, {3, 25.26}, {4, 64.60}, {5, 110.81}, {6,
  160.89}, {7, 213.22}, {8, 266.98}, {9, 321.71}, {10,
  377.15}}; (*beta=1*)
dataSBMBousse10 = {{2.2, 0}, {3, 43.32}, {4, 97.62}, {5, 152.25}, {6,
  207.27}, {7, 262.70}, {8, 318.52}, {9, 374.7}, {10,
  431.19}}; (*beta=10*)

SBMBousse014 = ListLinePlot[dataSBMBousse014, PlotStyle -> Black];
SBMBousse001 = ListLinePlot[dataSBMBousse001, PlotStyle -> Blue];
SBMBousse1 = ListLinePlot[dataSBMBousse1, PlotStyle -> Red];
SBMBousse10 =
  ListLinePlot[dataSBMBousse10, PlotStyle -> Darker[Green]];
g0 = ListPlot[datanul, PlotStyle -> White,

```

```

AxesLabel -> {"pH",
  "-!\(\(*SubscriptBox[\["[CapitalDelta]\[Psi]\", \("0\["\]) (mV)"}];
Show[g0, SBMBousse014, SBMBousse001, SBMBousse1, SBMBousse10]

```

A.2 Van Hal and Gouy-Chapman theory

```

Clear[Eq1, \[Psi]o, \[Sigma]o];
Kb = 10^2;
Ka = 10^-6;
Ns = 5*10^17;
q = 1.602*10^-19;
k = 1.3806*10^-23;
T = 300;
z = 1;
\[Epsilon]w = 80.0;
\[Epsilon]o = 8.854*10^-12;
AN = 6.022*10^23; (* # molecules moles^-1*)
Co = 0.1; (**(10^-3); Molar *)
n\[Infinity] = 1000* AN* Co;
pHb = { 2, 3, 4, 5.1, 6.1, 7.1, 8.1, 8.3, 8.31};
\[Sigma]o =
  Sqrt[8.0*k*T*\[Epsilon]w*\[Epsilon]o*n\[Infinity]]*
  Sinh[(z*q*\[Psi]o)/(2.0*k*T)];
Eq1 = -pHb -
  Log[10, (
    Kb*\[Sigma]o +
    Sqrt[(Kb*\[Sigma]o)^2 + 4*Ka*Kb*(q^2*Ns^2 - \[Sigma]o^2)]/(
    2.0*(q*Ns - \[Sigma]o))] - (q*\[Psi]o)/(2.3*k*T);

For[i = 1, i < 10, i++, Print[FindRoot[Eq1[[i]] == 0, {\[Psi]o, 1}]]]
datanul = {{0, 0}};
dataSBMGC1 = {{2, 0}, {3, 7.92}, {4, 31.06}, {5, 65.89}, {6,
  104.29}, {7, 143.35}, {8, 182.19}, {9, 220.14}, {10,
  255.98}}; (*Ns = 5 x 10^18 Co = 1 mM*)
dataSBMGC10 = {{2, 0}, {3, 3.05}, {4, 17.36}, {5, 47.51}, {6,
  84.48}, {7, 122.84}, {8, 160.68}, {9, 196.50}, {10,
  227.25}}; (*Ns = 5 x 10^18 Co = 0.01M*)
dataSBMGC100 = {{2, 0}, {3, 0}, {4, 7.99}, {5.1, 33.79}, {6.1,
  68.39}, {7.1, 105.20}, {8.1, 140.47}, {9.1, 170.37}, {10.1,
  188.34}}; (*Ns = 5 x 10^18 Co = 0.1M*)
dataSBMGCNs19 = {{2, 0}, {3, 7.9}, {4, 31.06}, {5.1, 69.65}, {6.1,
  108.19}, {7.1, 147.25}, {8.1, 186.03}, {9.1, 223.85}, {10.1,
  259.36}}; (*Ns =5 x 10^19 Co=0.1M*)
dataSBMGCNs17 = {{2, 0}, {3, 0.12}, {4, 1.05}, {5.1, 8.96}, {6.1,
  29.72}, {7.1, 55.03}, {8.1, 71.98}, {8.3, 73.72}, {8.31,
  73.79}}; (*Ns =5 x 10^17 Co=0.1M*)

```

```

g0 = ListPlot[datanul, PlotStyle -> White,
  AxesLabel -> {"pH",
    "-!\(\(*SubscriptBox[\\"[CapitalDelta]\[Psi]\", \\"0\"]\) (mV)"}];
SBMGC1 = ListLinePlot[dataSBMGC1, PlotStyle -> Black];
SBMGC10 = ListLinePlot[dataSBMGC10, PlotStyle -> Blue];
SBMGC100 = ListLinePlot[dataSBMGC100, PlotStyle -> Blue];
SBMGCNs19 = ListLinePlot[dataSBMGCNs19, PlotStyle -> Darker[Green]];
SBMGCNs17 = ListLinePlot[dataSBMGCNs17, PlotStyle -> Red];
Show[g0, SBMGC100, SBMGCNs19, SBMGCNs17]

```

A.3 Van Hal and Gouy-Chapman-Stern theory

```

Clear[Eq1, Eq2, \[Psi]o, \[Sigma]o];
Kb = 10^2;
Ka = 10^-6;
Ns = 5*10^17;
q = 1.602*10^-19;
k = 1.3806*10^-23;
T = 300;
z = 1;
\[Epsilon]w = 80.0;
\[Epsilon]o = 8.854*10^-12;
AN = 6.022*10^23; (* # molecules moles^-1*)
Co = 100.0*10^-3; (* Molar *)
n\[Infinity] = 1000 AN Co;
pHb = 5;
Cist = 0.8;
\[Psi]o = -0.207*10^-3;(*mV*)
(* For each \[Psi]o find \[Phi]2. Each \[Phi]2 find \[Sigma]o. Solve \
pHb with found params *)
Eq1 = -\[Psi]o + \[Phi]2 + (
  Sqrt[8.0*k*T*\[Epsilon]w*\[Epsilon]o*n\[Infinity]]*
  Sinh[(z*q*\[Phi]2)/(2.0*k*T)]/Cist;
S1 = FindRoot[Eq1 == 0, {\[Phi]2, 1}];
\[Sigma]o =
  Sqrt[8.0*k*T*\[Epsilon]w*\[Epsilon]o*n\[Infinity]]*
  Sinh[(z*q*\[Phi]2)/(2.0*k*T)] /. S1;
pHb = -Log[10, (
  Kb*\[Sigma]o +
  Sqrt[(Kb*\[Sigma]o)^2 + 4*Ka*Kb*(q^2*Ns^2 - \[Sigma]o^2)]/(
  2.0*(q*Ns - \[Sigma]o))] - (q*\[Psi]o)/(2.3*k*T)
datanul = { {0, 0}};
dataSBMGCS1 = {{2, 0}, {3.00072, 8.47}, {4.0001, 32.44}, {5.00009,
  68.51}, {6.0001, 109.26}, {7.0008, 152.47}, {8.00009,
  197.85}, {9.00019, 245.30}, {10.001,
  294.58}};(*C0=1mM en Ns = 5x10^18*)

```

```

dataSBMGCS10 = {{2, 0}, {3.00095, 3.82}, {4.0002, 20.19}, {5.00003,
    52.91}, {6.00018, 93.87}, {7.00004, 138.64}, {8.00018,
    185.92}, {9.00007, 235.1}, {10.0001,
    285.76}};(*C0=0.01M en Ns = 5x10^18*)
dataSBMGCS100 = {{2, 0}, {3.00066, 1.93}, {4.00049, 12.75}, {5.00001,
    41.20}, {6.0001, 81.53}, {7.00017, 127.34}, {8.00007,
    176.01}, {9.00002, 226.47}, {10.0002,
    278.17}};(*C0=0.1M en Ns = 5x10^18*)
dataGCS17 = {{2, 0}, {3.00146, 0.207}, {4.00169, 1.94}, {5.00018,
    12.29}, {6.00008, 38.35}, {7.00015, 73.68}, {8.00003,
    111.05}, {9.0003, 145.05}, {10,
    168.32}};(*C0=0.1M en Ns = 5x10^17*)
dataGCS19 = {{2, 0}, {3.00041, 12.57}, {4.00013, 41.45}, {5.00031,
    82.25}, {6.00013, 128.65}, {7.00005, 178.07}, {8.00002,
    229.43}, {9.00016, 282.17}, {10.0001,
    335.92}};(*C0=0.1M en Ns = 5x10^19*)
g0 = ListPlot[datanul, PlotStyle -> White,
    AxesLabel -> {"pH",
        "-!\(\*SubscriptBox[\[CapitalDelta][Psi]\", \"0\"]\) (mV)"}];
SBMGCS1 = ListLinePlot[dataSBMGCS1, PlotStyle -> Black];
SBMGCS10 = ListLinePlot[dataSBMGCS10, PlotStyle -> Red];
SBMGCS100 = ListLinePlot[dataSBMGCS100, PlotStyle -> Blue];
GCS17 = ListLinePlot[dataGCS17, PlotStyle -> Red];
GCS19 = ListLinePlot[dataGCS19, PlotStyle -> Darker[Green]];
Show[g0, SBMGCS1, SBMGCS10, SBMGCS100]
Show[g0, SBMGCS100, GCS17, GCS19]
    
```

Appendix B

List of parameters

A list of constants in this thesis, in alphabetical order:

| | | |
|------------------------|-------------------------|-------------------------------------|
| C_{stern} | Stern layer capacitance | $0.8 F$ |
| F | Faraday constant | $96485.3399 Cmol^{-1}$ |
| k | Boltzmann constant | $1.3806 \cdot 10^{-23} J/K$ |
| N_A | Avogadro's number | $6.02214179 \cdot 10^{23} mol^{-1}$ |
| q | atomic charge | $1.602 \cdot 10^{-19} C$ |
| R | gas constant | $8.314472 J/K^{-1}mol^{-1}$ |
| T | room temperature | $300 K$ |
| $\frac{1}{q}\Psi^{Si}$ | work function silicon | $4.7 V$ |

A list of all parameters and variables in this thesis, in alphabetical order:

| | | |
|-------------------|--|---------------|
| a_i | activity | |
| A_c | cross sectional area | m^2 |
| $a_{H_B^+}$ | proton activity in electrolyte bulk | |
| $a_{H_s^+}$ | proton activity near oxide surface | |
| B | number of basic groups | |
| C_{dif} | differential double layer capacitance | F |
| $C_{\text{dl},i}$ | integral double layer capacitance | F |
| C_i | insulator capacitance | F |
| c_i^0 | molar concentration of species i in bulk | mol |
| $c_i(x)$ | molar concentration of species i in bulk at distance x | mol |
| d_c | thickness of silicon | m |
| d_i | thickness of oxide | m |
| E_I | interface potential | V |
| E_{ref} | reference electrode voltage | V |
| f_i | activity coefficient | 1 |
| f_d | depletion function | |
| G_c | conductance of channel | Ω^{-1} |
| h | height of nanowire | m |
| i_{ds} | drain-source current | A |
| K_a | acidic equilibrium constant | |
| K_b | basic equilibrium constant | |

| | | |
|-----------------|--|------------|
| n^0 | number concentration of each ion in bulk | |
| N_a | doping concentration | mol^{-1} |
| N_s | number of surface sites | m^{-2} |
| pH_B | bulk pH | |
| pH_{pzc} | point of zero charge pH | |
| pH_s | surface pH | |
| Q_a | free ionised impurity charge in accumulation regime | C |
| Q_c | majority carrier charge per unit length | Cm^{-1} |
| Q_d | bound ionised impurity charge in depletion regime | C |
| Q_i | free ionised impurity charge in inversion regime | C |
| Q_m | mobile ionic charge | C |
| t_f | thickness of oxide | m |
| v | Bousse model term | |
| V | volume of bulk | m^3 |
| V_{ds} | drain source voltage | V |
| V_{fb} | flatband voltage | V |
| V_{fg} | frontgate voltage | V |
| V_{gs} | gate-source voltage | V |
| V_T | threshold voltage | V |
| w | width of nanowire | m |
| x_H | distance from surface | m |
| y_o | Bousse model term | |
| z | ion valence | $1 C$ |
| α_o | Bousse model term | |
| α | sensitivity parameter | |
| α | base angle | rad |
| β | sensitivity parameter | |
| β_{int} | intrinsic buffer capacity | |
| δ | reactivity insulator surface | |
| $\delta\chi$ | variations of χ potentials | V |
| ϵ_o | permittivity of free space | Fm^{-1} |
| ϵ_{ox} | permittivity of oxide | Fm^{-1} |
| ϵ_r | relative permittivity | |
| ϵ_{si} | permittivity of silicon | Fm^{-1} |
| μ_b | mobility of majority carriers | |
| ν_i | surface activity of species | i |
| χ^2 | fit test parameter | |
| χ^{sol} | surface dipole potential | V |
| σ_o | surface charge density | Cm^{-2} |
| σ_{dl} | charge in diffuse layer | Cm^{-2} |
| ψ_0 | potential difference oxide surface and bulk solution | V |
| ψ_B | bulk potential | V |
| ψ_H | potential at Helmholtz plane | V |
| ψ_s | potential oxide surface | V |

References

- [1] P. Bergveld, *De OSFET en de ISFET : veld-effekt transistor elektroden voor elektrofysiologische toepassingen*. PhD thesis, Technische Hogeschool Twente, 1973.
- [2] L. Bousse, N. de Rooij, and P. Bergveld, "Operation of chemically sensitive field-effect sensors as a function of the insulator-electrolyte interface," *IEEE Transactions on Electron Devices*, vol. 30, no. 10, pp. 1263–1270, 1983.
- [3] A. van den Berg, P. Bergveld, D. N. Reinhoudt, and E. J. R. Sudholter, "Sensitivity control of ISFETs by chemical surface modification," *Sensors and Actuators*, vol. 8, pp. 129–148, 1985.
- [4] R. van Hal, J. Eijkel, and P. Bergveld, "A general model to describe the electrostatic potential at electrolyte oxide interfaces," *Advances in colloid and interface science*, vol. 69, pp. 31–62, 1996.
- [5] S. Chen, J. G. Bommer, W. G. van der Wiel, E. T. Carlen, and A. van den Berg, "Top-down fabrication of sub-30 nm monocrystalline silicon nanowires using conventional microfabrication," *ACS Nano*, vol. 3, no. 11, pp. 3485–3492, 2009.
- [6] M. N. Masood, S. Chen, E. T. Carlen, and A. van den Berg, "All-(111) surface silicon nanowires: Selective functionalization for biosensing applications." Submitted 2010, 2010.
- [7] J.-F. Hsu, B.-R. Huang, C.-S. Huang, and H.-L. Chen, "Silicon nanowires as pH sensor," *Japanese Journal of Applied Physics*, vol. 44, pp. 2626–2629, 2005.
- [8] O. Knopfmacher, A. Tarasov, W. Fu, M. Wipf, B. Niesen, M. Calame, and C. Schönenberger, "Nernst limit in dual-gated si-nanowire FET sensors," *Nano Letters*, vol. 10, pp. 2268–2274, 2010.
- [9] Y. Cui, Q. Wei, H. Park, and C. M. Lieber, "Nanowire nanosensors for highly sensitive and selective detection of biological and chemical species," *Science*, vol. 293, pp. 1289–1292, 2001.
- [10] E. T. Carlen, "Nanowire electrochemical sensors: can we live without labels?," *Lab on a Chip*, vol. 7, pp. 19–23, 2007.
- [11] Y. L. Bunimovich, Y. S. Shin, W.-S. Yeo, M. Amori, G. Kwong, and J. R. Heath, "Quantitative real-time measurements of DNA hybridization with alkylated nonoxidized silicon nanowires in electrolyte solution," *Journal of the American Chemical Society*, vol. 128, pp. 16323–16331, 2006.
- [12] E. Stern, J. F. Klemic, D. A. Routenberg, P. N. Wyrembak, D. B. Turner-Evans, A. D. Hamilton, D. A. LaVan, T. M. Fahmy, and M. A. Reed, "Label-free immunodetection with CMOS-compatible semiconducting nanowires," *Nature*, vol. 445, pp. 519–522, 2007.
- [13] H. D. Tong, S. Chen, W. G. van der Wiel, E. T. Carlen, and A. van den Berg, "Novel top-down wafer-scale fabrication of single crystal silicon nanowires," *Nano Letters*, vol. 9, pp. 1015–1022, 2009.

- [14] D. E. Yates, S. Levine, and T. W. Healy, "Site-binding model of the electrical double layer at the oxide/water interface," *Journal of the Chemical Society, Faraday Transactions 1*, vol. 70, pp. 1807–1818, 1974.
- [15] P. Bergveld, "ISFET, theory and practice," *IEEE sensor conference Toronto*, vol. October, pp. 1–26, 2003.
- [16] N. Elfström, R. Juhasz, I. Sychugov, T. Engfeldt, A. Eriksson Karlström, and J. Linros, "Surface charge sensitivity of silicon nanowires: Size dependence," *Nano Letters*, vol. 7, pp. 2608–2612, 2007.
- [17] M. G. Nikolaides, S. Rauschenbach, and A. R. Bausch, "Characterization of a silicon-on-insulator based thin film resistor in electrolyte solutions for sensor applications," *Journal of Applied Physics*, vol. 95, pp. 3811–3815, 2004.
- [18] E. D. Minot, A. M. Janssens, I. Heller, H. A. Heering, C. Dekker, and S. Lemay, "Carbon nanotube biosensors: The critical role of the reference electrode," *Applied Physics Letters*, vol. 91, no. 9, pp. 093507 – 093507–3, 2007.
- [19] D. V. Vezenov, A. Noy, L. F. Rozsnyai, and C. M. Lieber, "Force titrations and ionization state sensitive imaging of functional groups in aqueous solutions by chemical force microscopy," *Journal of the Chemical Society*, vol. 119, pp. 2006–2015, 1997.
- [20] J. A. Davis, R. O. James, and J. O. Leckie, "Surface ionization and complexation at the oxide/water interface," *Journal of Colloid and Interface Science*, vol. 63, pp. 480–499, 1978.
- [21] S. Sze, *Physics of semiconductor devices*. John Wiley and sons, 1981.
- [22] D. C. Howell, "Chi-square test - analysis of contingency tables." Online, <http://www.uvm.edu/~dhowell/methods7/Supplements/ChiSquareTests.pdf>. Last accessed November 8, 2010.